Applied Catalysis B: Environmental 199 (2016) 224–229

Contents lists available at ScienceDirect

Applied Catalysis B: Environmental

journal homepage: www.elsevier.com/locate/apcatb

Optical band structure and photogenerated carriers transfer dynamics in FTO/TiO_2 heterojunction photocatalysts

Linpeng Jiang, Huiling Yu, Liyi Shi, Yin Zhao*, Zhuyi Wang, Meihong Zhang, Shuai Yuan*

Research Center of Nanoscience and Nanotechnology, Shanghai University, 99 Shangda Road, Shanghai 200444, PR China

ARTICLE INFO

Article history:
Received 8 April 2016
Received in revised form 25 May 2016
Accepted 28 May 2016
Available online 30 May 2016

Keywords:
FTO/TiO_2 heterojunction
Photocatalytic
Photoelectrocatalytic
Optical band structure
Carriers transfer dynamics

ABSTRACT

The FTO/TiO_2 heterojunction photocatalysts were prepared and characterized by XRD, SEM, UV–vis and electrochemical impedance measurement. The effect of F doping level on the optical band gap and conductivity of as-prepared FTO samples, as well as the band alignment of FTO/TiO_2 heterojunction photocatalyst was detailed analyzed. In addition, the change of optical band structure and conductivity caused by F doing was correlated with observed carriers transport properties including charge carriers separation, transport and interface transfer in the FTO/TiO_2 heterojunction photocatalyst. Finally, the photocatalytic activity, photoelectrocatalytic performance and their photocatalytic mechanism were systematically discussed. The primary results demonstrate that the heterojunction structure in the FTO/TiO_2 photocatalyst can effectively separate photogenerated carriers; however, the expense of redox ability is unavoidable. Among these, the FTO(1)/TiO_2 sample displays the highest photocatalytic activity, which is attributed to that the benefit of inhibiting recombination has dominant effect on photocatalytic performance.

1. Introduction

With the increasingly serious environmental pollution concerns, the heterogeneous photochemical reaction on semiconductor has become one of the most promising technologies because of its unique ability of environmental purification and energy conversion [1–3]. Generally, the wide gap semiconductor has been widely applied in photovoltaic fields due to its low cost, non-toxicity and good chemical stability, especially titanium dioxide (TiO_2) [1,3–6]. However, the unsatisfactory recombination of photo-generated hole-electron pairs in semiconductor greatly inhibits photoelectric conversion efficiency and limits its industrial application [2,3,7–9].

The process of coupling two kinds of semiconductor to form heterojunction structure has been employed to design new photocatalyst, due to its efficiency photogenerated charge carriers separation capacity before recombination [3,5,10–12]. However, the photogenerated electron-hole pairs driven by internal electric field within heterojunction structure still cannot avoid from the carriers recombination and the back-reaction of intermediate species [3]. The most valid strategy to mitigate such charge losses is to assemble a high-speed channel aiming for transporting carriers to the surface of photocatalysts timely and taking part in degradation reaction immediately.

Recently, carbon structure, as a high-performance conductive material, has been widely investigated with above strategy [4,8,13]. Yao et al. reported that carbon nanotube (CNTs)/TiO_2 composite material behaved faster charge separation ability, which showed nearly 2 times higher phenol degradation rate compared to the pure TiO_2 [14]. Zhang et al. observed that P25 nanoparticles loaded graphene nanosheet structure showed significant improvement in photodegradation of methylene blue since an excellent conductivity path formed [15]. However, carbon structure material generally shows deeper color, which may limit its photocatalytic performance due to its poor utilization of light. Therefore, the design of desired heterojunction photocatalyst system behaving excellent light utilization, photogenerated carriers separated and transport ability is needed.

Transparent conductive oxides (TCO), behaving low resistance ($R < 10^{-3}\ \Omega$ cm) and high transmittance brought by wide band gap (Eg > 3 eV) [1,9,16–18], have been used to fabricate the heterostructure photocatalysts. For instance, Shen et al. prepared the TiO_2/SnO_2 nanocrystalline sol behaving twice faster rhodamine B (RB) removing ability than that of pure TiO_2, since its better charge separation capacity [7]. Sher et al. reported that W-doped SnO_2 (TTO)/TiO_2 displayed a significantly high photocatalytic in removing gaseous 2-propanol (IP) under visible-light irradiation attribute to its inter-semiconductor hole-separation between TTO and TiO_2

* Corresponding authors.
E-mail addresses: zhaoyin@shu.edu.cn, zhaoyinsunny@163.com (Y. Zhao), s.yuan@shu.edu.cn (S. Yuan).

http://dx.doi.org/10.1016/j.apcatb.2016.05.070
0926-3373/

[19]. Generally, doping impurity atom is a widely adopted method to improve the conductivity of TCO material, owning to produces more free charges. Meanwhile, the introduction of impurity atom inevitably alters the optical band structure of TCO materials. Despite some research focus on the TCO/TiO_2 heterojunction photocatalystic system, the detail investigation about physicochemical properties of TCO/TiO_2 heterojunction photocatalyst with different impurity doing level, interrelated charge carriers transmission behavior, and its photocatalytic mechanism is still desired to understand.

Herein, the FTO/TiO_2 heterojunctions photocatalyst film was achieved via mixing TiO_2 and FTO crystal with different F doping level. Meanwhile, the optical band gap and band alignment of FTO/TiO_2 heterojunction photocatalyst film were evaluated by UV–vis and Mott-Shottky (MS) analysis. Additional, the effect of optical band structure and conductive property of FTO/TiO_2 heterojunction photocatalyst film on the carriers transport properties including charge carriers separate, transport, and interface transfer were detailed studied by electrochemical impedance measurement (EIS). Finally, the photocatalytic activity, photoelectrocatalytic performance and their mechanism were systematically discussed.

2. Experimental

2.1. Preparation of FTO/TiO_2 heterojunctions photocatalyst

TiO_2 (P25) was purchased from Degussa Corp. The FTO sols were synthesized by sol–gel process followed by a hydrothermal treatment, according to our previous work [20]. Firstly, two kinds of ethyl cellulose (EC, Sigma Aldrich) with different viscosity (5–15 mPa s and 30–60 mPa s) were dissolved in 20 mL ethanol in advance. 1.06 g EC (5–15 mPa s) and 0.82 g EC (30–60 mPa s) of this ethanol solution was then mixed with 3.75 g of FTO/TiO_2 nanoparticles powders (weight proportions of FTO and TiO_2 is 50:100) and 18.21 g α-terpineol (anhydrous, 90%, Sigma – Aldrich) in round bottomed rotavap flask. After that, this mixture was sonicated for 15 min and stirred for 3 h by hand for three consecutive times. Followed by rotary evaporation at 30 °C, 68 r.p.m. The paste was finally achieved with grinding by mortar grinder at 5 daN longitudinal and 20 daN lateral pressure (FRITSCH, Germany) for 30 min.

Then, the paste was spread on the conductive glass by screen printing method, and dried at room temperature for at least 30 min. After that, the electrode was sintered in an oven at 450 °C for 30 min. Finally, the FTO/TiO_2 photocatalyst film was obtained. In present study, FTO(x)/TiO_2 is corresponding to the samples, and the x was represented the molar content of fluoride in FTO. Meanwhile, the corresponding pure TiO_2 and different F doping FTO films (named as sample FTO(0), sample FTO(1), sample FTO(2)) were prepared in the same way.

2.2. Characterization methods

Wide-angel X-ray diffraction measurements were carried out in grazing angle pattern ($\omega = 2^\circ$, $2\theta = 20^\circ$–80°) using a PANalytical X-ray diffractometer (Cu Kα radiation 40 kV, 40 mA). The morphology observation of FTO/TiO_2 photocatalyst film was verified by electron microscopy (SEM) on JEOL JSM-700F. Sheet resistances were characterized by the standard four-probe method (SDY-5 four-point probe meter). Fluorine content in FTO was understood by ion-selective electrode method using PF-1C (201) fluoride ion electrode instrument. The diffuse absorption spectras over a range of 200–700 nm were recorded by Shimadzu UV-2450/2550 with an integrating sphere using $BaSO_4$ as a reference. The photoelectric performance was measured using an electrochemical system (CHI-760E, Chenhua Instruments, Shanghai, China). A standard three-electrode system with as-prepared 2 cm^2 active area photocatalyst films, a platinum sheet counter electrode and Ag/AgCl reference electrode was used in those photoelectric study. In addition, 1 M KOH was used as the electrolyte solution. And a 500 W Xe lamp was used as the light source and positioned 19 cm away from the as-prepared photocatalyst film.

2.3. Photocatalytic activity measurement

The photocatalytic activity was evaluated by the degradation of methylene blue (MB). The prepared samples were immersed in

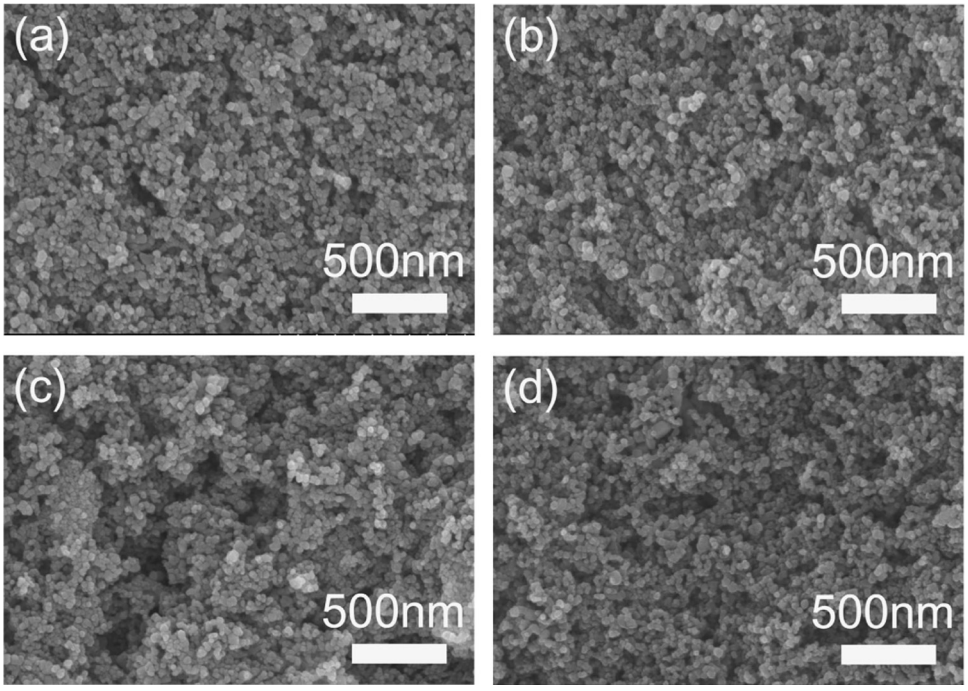

Fig. 1. SEM images of (a) pure TiO_2, (b) FTO(0)/TiO_2, (c) FTO(1)/TiO_2 and (d) FTO(2)/TiO_2 heterojunction photocatalyst.

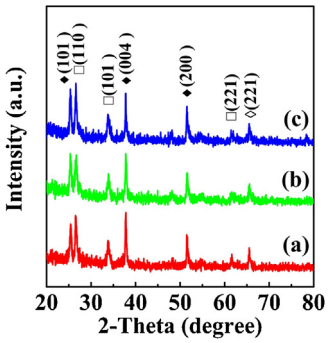

Fig. 2. XRD pattern of (a) FTO(0)/TiO_2, (b) FTO(1)/TiO_2 and (c) FTO(2)/TiO_2 heterojunction photocatalyst film: anatase TiO_2 (♦), rutile TiO_2 (◊) and rutile SnO_2 (□).

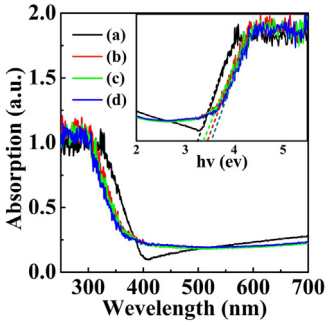

Fig. 3. UV–vis diffuse reflectance of (a) pure TiO_2, (b) FTO(0)/TiO_2, (c) FTO(1)/TiO_2 and (d) FTO(2)/TiO_2 heterojunction photocatalyst. The inset is the corresponding the plots for the band gap energy (Eg).

50 mL aqueous MB (6.0 mg/L). After stirring under dark for 60 min, the catalytic system was irradiated by UV light (GE, F8T5/BLB, 16 W, max = 365 nm). After a given irradiation time, the MB solution was withdrawn for subsequent analysis using UV–vis spectrophotometer (Lengguang Tech co. let. Gold S54T). The efficiency of degradation was calculated from formula (1) as follows:

$$\text{Degradation Rate}\,(\%) = \left(\frac{C_0 - C}{C_0}\right) \times 100\% \quad (1)$$

where C_0 and C are the original MB concentration after the adsorption/desorption reached equilibrium and residual MB concentration after reaction, respectively. According to photoelectrocatalytic activity, 1 V basis potential (controlled by Instek, GPS2303C) was applied in the same photocatalytic evaluation process.

3. Result and discussion

The morphology and phase structure of pure TiO_2 and as-prepared FTO/TiO_2 photocatalyst films were characterized by field emission scanning electron (SEM) and X-ray diffraction (XRD). As shown in the high magnification of SEM images (as shown in Fig. 1), the pure TiO_2 and as-prepared FTO/TiO_2 photocatalyst films all exhibit homogeneous porous structures with plenty of tightly linked spheres. The EDX element mapping of all as-prepared FTO/TiO_2 photocatalyst films (as shown in Fig. S1) show that Ti, Sn and F elements are uniform dispersed in the plane. The XRD patterns of pure TiO_2 and as-prepared FTO/TiO_2 photocatalyst films are showed in Fig. 2. All the patterns display the same characteristic peaks which can be identified to TiO_2 (anatase: JCPDS #21-1272, rutile: JCPDS #21-1276) and SnO_2 (JCPDS #41-1445) [16], no characteristic peak for impurity is observed.

The optical band gap and band alignment of FTO/TiO_2 heterojunction photocatalyst film were evaluated by UV–vis spectra and electrochemical impedance spectroscopy. The UV–vis absorption spectra of pure TiO_2 and as-prepared FTO samples with different F doping level are showed in Fig. 3, and corresponding band gap energy (in the inset of Fig. 3) are calculated by following formula [21]:

$$(\alpha h\nu)^{1/n} = A\left(h\nu - E_g\right) \quad (2)$$

where α, ν and A are absorption coefficient, light frequency and a constant, respectively, n = 1/2 as the direct transition absorption coefficient. As shown, the Eg of pure TiO_2 is 3.27 eV, which is similar with the reported value of 3.2 eV [2,10]. The Eg value of sample FTO(0), sample FTO(1) and sample FTO(2) are 3.44, 3.37 and 3.52 eV, respectively.

To determine the relative band edge positions between pure TiO_2 and as-prepared FTO with different F doping level, the band edge positions of the conduction band (E_{CB}) and valence band (E_{VB}) of the two semiconductors at the point of zero charge is theoretically predicted using the following empirical equation [3,11,22]:

$$E_{CB} = \chi - E^e - 0.5E_g \quad (3)$$

$$E_{VB} = E_g - E_{CB} \quad (4)$$

Here, E_g is the band gap of pure TiO_2 (3.27 ev), sample FTO(0) (3.44 eV), sample FTO(1) (3.37 eV) and sample FTO(2) (3.52 eV) obtained in UV–vis measurement; E^e is the energy of free electrons on the hydrogen scale (4.5 eV). *X* is the Sanderson electronegativity of the semiconductor, which is defined as the geometric mean of the Muiliken electronegativities the atoms [22]. Specifically, the bulk electronegativity of an oxide (M_mO_n) is calculated by $\chi_{oxide} = \left[(\chi_M)^m(\chi_O{}^n)\right]^{1/(m+n)}$. For the as-prepared FTO samples, the actual chemical molecular formula of sample FTO(0), sample FTO(1) and sample FTO(2) measured by ion-selective electrode method is SnO_2, $SnO_{1.94}F_{0.06}$, $SnO_{1.90}F_{0.10}$, respectively. As a result, the *X* values of sample FTO(0), sample FTO(1) and sample FTO(2) are therefore 6.25, 6.29 and 6.32 eV, respectively. As well as, the calculated *X* value of TiO_2 is 5.81 eV which is similar with the values of as reported [3,17]. The calculated CB and VB edge of pure TiO_2 are −0.33 and 2.95 eV. For the as-prepared FTO samples, the calculated CB value is 0.03, 0.11 and 0.06 eV for sample FTO(0), sample FTO(1) and sample FTO(2), respectively. The corresponding valence band edge of sample FTO(0), sample FTO(1) and sample FTO(2) is 3.47, 3.48 and 3.58 eV, respectively.

In order to further address the relative band structure of pure TiO_2 and as-prepared FTO samples, the flat-band potentials were analyzed by using electrochemical impedance spectroscopy along with the Mott–Schottky (MS) equation [23]:

$$\frac{1}{C_x^2} = -\frac{2}{e\varepsilon_0 kNA^2}\left(E_{app} - E_{fb} - \frac{K_B T}{e}\right) \quad (5)$$

where e, ε_0, k, N, and A are the fundamental charge constant, vacuum permittivity, dielectric constant, density of donors within the space charge region, and effective surface area of the semiconductor. The MS plots of pure TiO_2 and as-prepared FTO samples in the aqueous solution of 1 M KOH are shown in Fig. 4. From the positive slope, it can be confirmed that all samples possessed a nature of n-type semiconductor. Moreover, the flat band potential can be calculated from the x-intercept of the linear portion of the MS data. It can be seen that the E_{fb} of all as-prepared FTO samples are more positive than the pure TiO_2. Specifically, the E_{fb} of pure TiO_2, sample FTO(0), sample FTO(1) and sample FTO(2) are 0.17, 0.67, 0.83 and 0.78 V (vs NHE), respectively. These results show the same trend as the result of theoretical calculation of CB value.

From the theoretical prediction (UV–vis measurement) and experimental analysis (MS analysis), the band alignment of FTO/TiO_2 photocatalyst can be portrayed in Fig. 7(b). As shown,

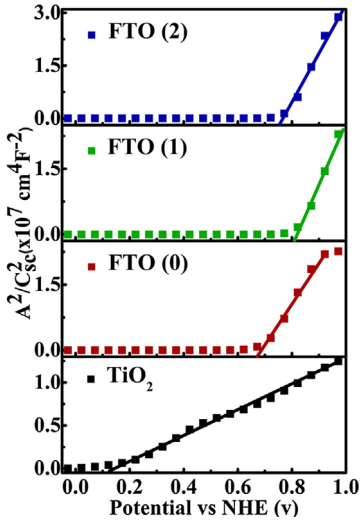

Fig. 4. Mott-Schottky plots for pure TiO_2 and as-prepared FTO samples.

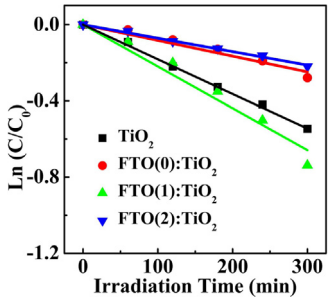

Fig. 5. The photocatalytic degradation of pure TiO_2 and FTO/TiO_2 heterojuction photocatalyst.

TiO_2 expresses higher CB and lower VB than that of all prepared FTO samples. The formation of the schottky barrier between TiO_2 and FTO would result in separation of photogenerated charge carriers [24].

The photocatalytic performance of pure TiO_2 and as-prepared FTO/TiO_2 photocatalyst are displayed in Fig. 5. Pseudo-first-order kinetics is assumed to calculate the corresponding degradation rate constant (k_{app}) [25]:

$$\mathrm{Ln}\left(\frac{C}{C_0}\right) = k \times t \quad (6)$$

where C_0 is the original MB concentration after the adsorption reached equilibrium (mg/L), C is the concentration (mg/L) at a given time t (min) and k_{app} is the first-order degradation rate constant (min^{-1}). The degradation rate and obtained k_{app} data list in Table 2. From Table 2, it can be observed that the k_{app} is 0.00177, 0.00092, 0.00219 and 0.00071 min^{-1} for pure TiO_2, sample FTO(0)/TiO_2, sample FTO(1)/TiO_2 and sample FTO(2)/TiO_2, respectively. The efficiencies of the sample FTO(1)/TiO_2 are higher than that of pure TiO_2, which shows the maximum photocatalytic activity.

In order to clear the factors affecting the photocatalytic performance, the photochemical behaviors such as charge carriers separate, transport, and interface transfer were studied using electrochemical impedance spectroscopy. Fig. 6 illustrates the Nyquist plots of the pure TiO_2 and as-prepared FTO/TiO_2 photocatalyst under irradiation at open-circuit potential. The corresponding parameters obtained from the equivalent circuit [26,27] (as shown in Fig. S2) via non-linear least square analysis software (ZView software) were fitted and listed in Table 1, where R_s is the electrolyte solution resistance, C_{sc} and R_t is respectively space charge capacitance and charge transport resistance related to the high frequency regime (10^4–10^5 H_Z) information in plot, C_d is the constant phase element for double layer capacitance and R_{tr} is interfacial charge transfer resistance across the electrode/electrolyte interface, which can be given by the low frequency regime information.

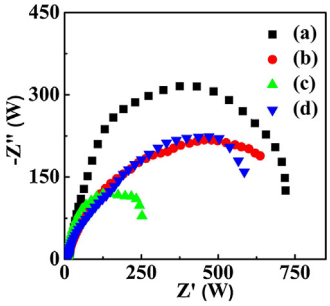

Fig. 6. The Nyquist plots of pure TiO_2 and FTO/TiO_2 heterojunction photocatalyst under light irradiation with open-circuit potential.

Table 1
The fitting results of EIS of as prepared TiO_2 and FTO/TiO_2 heterojunction photocatalyst.

Sample	R_s (Ω)[a]	C_{sc} (μF)[b]	R_t (Ω)[c]	C_d (μF)[d]	R_{tr} (Ω)[e]
Pure TiO_2	7.9	10.2	4.8	1416	787.9
FTO(0)/TiO_2	10.2	33.5	0.8	749	923.6
FTO(1)/TiO_2	9.0	93.1	0.7	3922	283.6
FTO(2)/TiO_2	9.8	16.9	0.6	1864	889.6

[a] The electrolyte solution resistance.
[b] The space charge capacitance, behaved build-in electric fields in FTO/TiO_2.
[c] The charge transport resistance inside the film.
[d] The constant phase element to represent the double layer capacitance across the electrode/electrolyte interface.
[e] Interfacial charge transfer resistance across the electrode/electrolyte interface.

Table 2
The photocatalystic and photoelectrocatalystic degradation rate and kinetic values of as prepared TiO_2 and FTO/TiO_2 heterojunction photocatalyst.

Sample	Photocatalysis (PC)		Photoelectrocatalysis (PEC)		Δ (%)[c]
	DR (%)[a]	K_{app} (min^{-1})[b]	DR (%)[a]	K_{app} (min^{-1})[b]	
Pure TiO_2	42.0	0.00177	46.2	0.00178	10.0
FTO(0)/TiO_2	28.2	0.00092	40.5	0.00146	43.4
FTO(1)/TiO_2	55.5	0.00219	88.8	0.00623	60.1
FTO(2)/TiO_2	22.6	0.00071	42.1	0.00130	86.3

[a] Degradation rate.
[b] First-order degradation rate constant.
[c] $\Delta = \frac{\text{Degradation rate}_{PEC} - \text{Degradation rate}_{PC}}{\text{Degradation rate}_{PC}} \times 100\%$.

As shown in Table 1, all FTO/TiO_2 photocatalyst express higher space charges capacitance (C_{sc}) than that of pure TiO_2. Among them, the sample FTO(1)/TiO_2 behaves highest C_{sc}. This is due to the fact that FTO/TiO_2 heterojunction photocatalyst forms build-in electric fields for easy separation of photogenerated carriers, especially for sample FTO(1)/TiO_2 with highest schottky barrier(supported by optical band structure analysis), which can more effectively weaken photogenerated carriers recombination.

With regard to charge transport properties, all as-prepared FTO/TiO_2 photocatalyst show lower R_t than that of pure TiO_2. Specifically, the order of Rt value is pure TiO_2 > sample FTO(0)/TiO_2 > sample FTO(1)/TiO_2 > sample FTO(2)/TiO_2. In our work (Fig. S3), the sheet resistance value of sample FTO(0), sample FTO(1), sample FTO(2) are 275, 125, 110 Ω/□ (the sheet resistance of pure TiO_2 is 579.7 kΩ/□), respectively. Clearly, the increasing conductive property of as-prepared FTO samples with increasing F doping level enhanced the charge transport ability of FTO/TiO_2 heterojunction photocatalyst.

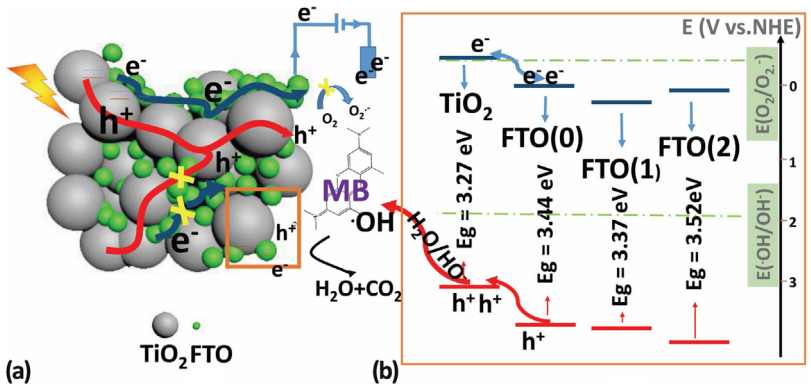

Fig. 7. Mechanism diagram: (a) photogenerated carriers transport mechanism in photocatalytic film (b) energy band alignment of as-prepared FTO/TiO_2 heterojunction photocatalyst.

In addition, the photogenerated carriers charge transfer characteristics across the electrode/electrolyte interface is studied. As shown in Table 1, sample FTO(1)/TiO_2 exhibits highest C_d and lowest R_{tr} compared with pure TiO_2 and other FTO/TiO_2 samples, which means the fastest interfacial charge transfer ability. This result can be explained that sample FTO(1)/TiO_2 possesses the highest build-in electric fields for driving separation of photogenerated carriers and excellent conductivity for transporting electron, resulting in the decrease of the charge recombination and then enhancement of interface charge transfer.

Attributing to the strong internal field, excellent internal charge transport and interfacial transfer ability, it is understandable that sample FTO(1)/TiO_2 endows the highest photocatalytic activity. However, the unexpected results is sample FTO(0)/TiO_2 and sample FTO(2)/TiO_2 show lower photocatalytic activity than that of pure TiO_2, although they have relatively prominent photoelectrochemical properties. Thus, the photocatalysis mechanism needs detailed analysis.

Based on the obtained optical band structure of pure TiO_2 and as-prepared FTO samples in our work (Fig. 7(b)), the photogenerated holes in as-prepared FTO sample can transfer easily to the valance band of pure TiO_2. These strongly oxidative valence band holes not only involve pollutant destruction, in turn, originate •OH radical in the presence of either adsorbed H_2O or the OH^- groups on the photocatalyst surface [2,11]. According to photogenerated electrons, the electrons in pure TiO_2 can migrate to the conduction band of as-prepared FTO sample. But the CB potential of all as-prepared FTO samples with different F doping level are more positive than the standard redox potential $E^0(O_2/{}^\bullet O_2^-$, −0.33 V) [11], which limited that the electrons (accumulated in the CB of FTO) are available for the generation of highly reactive hydroxyl radicals (•OH) and secondary oxidants ($HO_2^\bullet$, H_2O_2). Consequently, only moderately reductive conduction band electrons can participate in the photocatalytic degradation process. Clearly, the heterojunction structure in the FTO/TiO_2 photocatalyst can effectively separate of photogenerated carriers; however, the expense of redox ability is unavoidable. Compared with sample FTO(0)/TiO_2 and sample FTO(2)/TiO_2, the benefit of inhibiting recombination in sample FTO(1)/TiO_2 has dominant effect on photocatalytic performance. Thus, sample FTO(1)/TiO_2 displays the highest photocatalytic activity.

Furthermore, another interesting finding in our work is the charge transport resistance of all FTO/TiO_2 heterojunction photocatalyst is lower by more than an order of magnitude compared with pure TiO_2. We believe that these excellent photogenerated carriers transport properties certainly play a prominent role in photoelectrochemical synergistic catalysis process. Subsequently, the photoelectrocatalytic activity of pure TiO_2 and as-prepared FTO/TiO_2 photocatalyst was evaluated and the results list in Table 2. Compared with photocatalytic degradation results, the percentage of growth of degradation rate under UV light irradiation with the application of a controlled anodic potential through the supported catalyst is 10.0, 43.4, 60.1 and 86.3% for pure TiO_2, sample FTO(0)/TiO_2, sample FTO(1)/TiO_2 and sample FTO(2)/TiO_2, respectively. As Fig. 7(a) shown, when bias potential is applied to the FTO/TiO_2 photocatalyst film, the electrons accumulated in CB of FTO can be drove to the cathodic direction. In this process, the conductivity ability of electron transport channel forming by FTO in the heterojunction photocatalyst film makes a great contribution to the electron transport efficiency. To be specific, high conductivity ability of FTO can accelerate the electron transport inside the photocatalyst film, and then quicken the electron's transferring to cathodic direction under applying bias potential. Consequently, the recombination opportunity of photogenerated electron-hole pairs in FTO/TiO_2 heterostructures can be well reduced and the corresponding MB degradation can be improved [22,25]. In addition, the structure of conducting channel formed by as-prepared FTO samples is another determinant factor on photocatalytic or photoelectrocatalytic performance. As shown in proposed Fig. 7(a), the photogenerated holes and electrons accumulate in pure TiO_2 and as-prepared FTO channel, respectively. Too much or too little TiO_2 (or FTO) can not only effect on charge separation ability, but on the holes and electrons transport properties. In our work, the optimal as-prepared FTO sample content is 50 wt% (as shown in SI, Fig. S4). In summary, the design of desired heterojunction photocatalyst system behaving excellent light utilization, carrier separated and transport ability must comprehensively considered the optical band gap, conductivity properties, structure of band alignment and transport channel of each part in the heterojunction photocatalyst system.

4. Conclusion

The FTO/TiO_2 heterostructure photocatalyst with different F doping level is successfully prepared. The effect of optical band structure and conductivity of the FTO/TiO_2 heterostructure photocatalyst on the carriers transport properties, and correlated with observed photocatalytic and photoelectrocatalytic performance were detailed investigated. The major conclusions can be drawn: (i) all FTO/TiO_2 heterojunction photocatalytic systems form build-in electric fields for more easy separation of photogenerated carriers than that of pure TiO_2, (ii) sample FTO(1)/TiO_2 with highest schottky barrier can more effectively weaken carriers recombination, (iii) the order of R_t value is pure TiO_2 > sample FTO(0)/TiO_2 > sample FTO(1)/TiO_2 > sample FTO(2)/TiO_2, which is matched the conductive property of as-prepared FTO samples, (iv) the heterojunction

structure in the FTO/TiO_2 photocatalyst can effectively separate photogenerated carriers; however, the expense of redox ability is unavoidable, (vi) the benefit of inhibiting recombination in sample FTO(1)/TiO_2 has dominant effect on interfacial charge transfer ability, and then photocatalytic performance, (vii) the higher conductivity properties of as-prepared FTO lead to the higher increment of photoelectrocatalytic degradation rate of FTO/TiO_2 heterojunction photocatalyst, (viii) the structure of transport channel formed by as-prepared FTO is another determinant factor on photocatalytic performance, the optimal FTO content is 50 wt%.

Acknowledgement

The authors acknowledge the supports of National Natural Science Foundation of China (51302164, 51472154, 51202138 and 51202140), Natural Science Foundation of Shanghai (13ZR1417100, 12ZR1410500). Shanghai Municipal Science and Technology Commission (13DZ2292100), Baoshan District Science and Technology Commission of Shanghai (bkw2013142), Professional and Technical Service Platform for Designing and Manufacturing of Advanced Composite Materials, Shanghai, Science and Technological Program for Dongguan's Higher Education, Science and Research, and Health Care Institutions (2012108101014).

Appendix A. Supplementary data

Supplementary data associated with this article can be found, in the online version, at http://dx.doi.org/10.1016/j.apcatb.2016.05.070.

References

[1] J. Yuan, X. Zhang, H. Li, K. Wang, S. Gao, Z. Yin, H. Yu, X. Zhu, Z. Xiong, Y. Xie, TiO_2/SnO_2 double-shelled hollow spheres-highly efficient photocatalyst for the degradation of rhodamine B, Catal. Commun. 60 (2015) 129–133.
[2] F. Kayaci, S. Vempati, C. Ozgit-Akgun, I. Donmez, N. Biyikli, T. Uyar, Selective isolation of the electron or hole in photocatalysis: ZnO-TiO_2 and TiO_2-ZnO core-shell structured heterojunction nanofibers via electrospinning and atomic layer deposition, Nanoscale 6 (2014) 5735–5745.
[3] J. Yan, G. Wu, N. Guan, L. Li, Nb_2O_5/TiO_2 heterojunctions: synthesis strategy and photocatalytic activity, Appl. Catal. B: Environ. 152–153 (2014) 280–288.
[4] Z.-M. Yang, G.-F. Huang, W.-Q. Huang, J.-M. Wei, X.-G. Yan, Y.-Y. Liu, C. Jiao, Z. Wan, A. Pan, Novel Ag_3PO_4/CeO_2 composite with high efficiency and stability for photocatalytic applications, J. Mater. Chem. A 2 (2014) 1750–1756.
[5] A. Hamrouni, N. Moussa, F. Parrino, A. Di Paola, A. Houas, L. Palmisano, Sol–gel synthesis and photocatalytic activity of ZnO–SnO_2 nanocomposites, J. Mol. Catal. A: Chem. 390 (2014) 133–141.
[6] S. Sood, S.K. Mehta, A.S.K. Sinha, S.K. Kansal, Bi_2O_3/TiO_2 heterostructures: synthesis, characterization and their application in solar light mediated photocatalyzed degradation of an antibiotic, ofloxacin, Chem. Eng. J. 290 (2016) 45–52.
[7] S. Qianhong, Y. Hui, X. Qiang, Z. Yang, H. Rong, In-situ preparation of TiO_2/SnO_2 nanocrystalline sol for photocatalysis, Mater. Lett. 64 (2010) 442–444.
[8] H. Sun, S. Liu, S. Liu, S. Wang, A comparative study of reduced graphene oxide modified TiO2, ZnO and Ta_2O_5 in visible light photocatalytic/photochemical oxidation of methylene blue, Appl. Catal. B: Environ. 146 (2014) 162–168.
[9] X. Sun, H. Zhang, J. Wei, Q. Yu, P. Yang, F. Zhang, Preparation of point-line Bi_2WO_6@TiO_2 nanowires composite photocatalysts with enhanced UV/visible-light-driven photocatalytic activity, Mater. Sci. Semicond. Process. 45 (2016) 51–56.
[10] S. Bera, S.B. Rawal, H.J. Kim, W.I. Lee, Novel coupled structures of $FeWO_4$/TiO_2 and $FeWO_4$/TiO_2/CdS designed for highly efficient visible-light photocatalysis, ACS Appl. Mater. Interfaces 6 (2014) 9654–9663.
[11] N. Boonprakob, N. Wetchakun, S. Phanichphant, D. Waxler, P. Sherrell, A. Nattestad, J. Chen, B. Inceesungvorn, Enhanced visible-light photocatalytic activity of g-C_3N_4/TiO_2 films, J. Colloid Interface Sci. 417 (2014) 402–409.
[12] Y.C. Zhang, L. Yao, G. Zhang, D.D. Dionysiou, J. Li, X. Du, One-step hydrothermal synthesis of high-performance visible-light-driven SnS_2/SnO_2 nanoheterojunction photocatalyst for the reduction of aqueous Cr(VI), Appl. Catal. B: Environ. 144 (2014) 730–738.
[13] Y. Wang, Y.N. Zhang, G. Zhao, H. Tian, H. Shi, T. Zhou, Design of a novel Cu_2O/TiO_2/carbon aerogel electrode and its efficient electrosorption-assisted visible light photocatalytic degradation of 2,4,6-trichlorophenol, ACS Appl. Mater. Interfaces 4 (2012) 3965–3972.
[14] Y. Yao, G.h. Li, S. Ciston, R.M. Lueptow, K.A. Gray, Photoreactive TiO_2/carbon nanotube composites: synthesis and reactivity, Environ. Sci. Technol. 42 (2008) 4952–4957.
[15] H. Zhang, X.J. Lv, Y.M. L, Y. Wang, J.H. Li, P25-graphene composite as a high performance photocatalyst, ACS Nano 4 (2010) 380–386.
[16] R. Sasikala, A. Shirole, V. Sudarsan, T. Sakuntala, C. Sudakar, R. Naik, S.R. Bharadwaj, Highly dispersed phase of SnO_2 on TiO_2 nanoparticles synthesized by polyol-mediated route: photocatalytic activity for hydrogen generation, Int. J. Hydrogen Energy 34 (2009) 3621–3630.
[17] Z. Yang, S. Gao, T. Li, F.Q. Liu, Y. Ren, T. Xu, Enhanced electron extraction from template-free 3D nanoparticulate transparent conducting oxide (TCO) electrodes for dye-sensitized solar cells, ACS Appl. Mater. Interfaces 4 (2012) 4419–4427.
[18] S. Park, C.W. Lee, I.S. Cho, S. Kim, J.H. Park, H.J. Kim, D.-W. Kim, S. Lee, K.S. Hong, Growth of anatase and rutile TiO_2@Sb:SnO_2 heterostructures and their application in photoelectrochemical water splitting, Int. J. Hydrogen Energy 39 (2014) 17508–17516.
[19] S.B. Rawal, D.P. Ojha, Y.S. Choi, W.I. Lee, Coupling of W-doped SnO_2 and TiO_2 for efficient visible-light photocatalysis, Bull. Korean Chem. Soc. 35 (2014) 913–918.
[20] S. Wu, S. Yuan, L. Shi, Y. Zhao, J. Fang, Preparation, characterization and electrical properties of fluorine-doped tin dioxide nanocrystals, J. Colloid Interface Sci. 346 (2010) 12–16.
[21] X. Guo, W. Di, C. Chen, C. Liu, X. Wang, W. Qin, Enhanced near-infrared photocatalysis of $NaYF_4$:Yb, Tm/CdS/TiO_2 composites, Dalton Trans. 43 (2014) 1048–1054.
[22] L. Li, P.A. Salvador, G.S. Rohrer, Photocatalysts with internal electric fields, Nanoscale 6 (2014) 24–42.
[23] G. Natu, P. Hasin, Z. Huang, Z. Ji, M. He, Y. Wu, Valence band-edge engineering of nickel oxide nanoparticles via cobalt doping for application in p-type dye-sensitized solar cells, ACS Appl. Mater. Interfaces 4 (2012) 5922–5929.
[24] H. Wang, L. Zhang, Z. Chen, J. Hu, S. Li, Z. Wang, J. Liu, X. Wang, Semiconductor heterojunction photocatalysts: design, construction, and photocatalytic performances, Chem. Soc. Rev. 43 (2014) 5234–5244.
[25] M. Zhang, S. Yuan, Z.Y. Wang, Y. Zhao, L.Y. Shi, Photoelectrocatalytic properties of Cu^{2+}-doped TiO_2 film under visible light, Appl. Catal. B: Environ. 134–135 (2013) 185–192.
[26] G. Jiang, Z. Lin, L. Zhu, Y. Ding, H. Tang, Preparation and photoelectrocatalytic properties of titania/carbon nanotube composite films, Carbon 48 (2010) 3369–3375.
[27] J. Lin, R. Zong, M. Zhou, Y. Zhu, Photoelectric catalytic degradation of methylene blue by C60-modified TiO_2 nanotube array, Appl. Catal. B: Environ. 89 (2009) 425–431.